The effective point of measurement for depth-dose measurements in small MV photon beams with different detectors

Sonja Wegener[a], and Otto A. Sauer
Radiation Oncology, University of Wuerzburg, Josef-Schneider-Str. 11, 97080 Wuerzburg, Germany

(Received 19 December 2018; revised 11 July 2019; accepted for publication 6 August 2019; published 17 September 2019)

Purpose: The effective point of measurement (EPOM) of cylindrical ionization chambers differs from their geometric center. The exact shift depends on chamber construction details, above all the chamber size, and to some degree on the field-size and beam quality. It generally decreases as the chamber dimensions get smaller. In this work, effective points of measurement in small photon fields of a range of cylindrical chambers of different sizes are investigated, including small chambers that have not been studied previously.
Methods: In this investigation, effective points of measurement for different ionization chambers (Farmer type, scanning chambers, micro-ionization chambers) and solid state detectors were determined by measuring depth-ionization curves in a 6 MV beam in field sizes between 2 × 2 cm^2 and 10 × 10 cm^2 and comparing those curves with curves measured with plane-parallel chambers.
Results: It was possible to average the results to one shift per detector, as the results were sufficiently independent of the studied field sizes. For cylindrical ion chambers, shifts of the EPOM were determined to be between 0.49 and 0.30 times the inner chamber radius from the reference point.
Conclusions: We experimentally confirmed the previously reported decrease of the EPOM shift with decreasing detector size. Highly accurate data for a large range of detectors, including new very small ones, were determined. Thus, small chambers noticeably differ from the 0.5-times to 0.6-times the inner chamber radius recommendations in current dosimetry protocols. The detector-individual EPOMs need to be considered for measurements of depth-dose curves. [https://doi.org/10.1002/mp.13788]

Key words: depth dose curves, effective point of measurement, ionization chambers, micro-chambers

1. INTRODUCTION

When an air-filled ionization chamber is placed in water, some of the medium in the chamber cavity is replaced with air. This can be accounted for with a displacement correction factor or by shifting the chamber position from the central axis to a point — the effective point of measurement (EPOM) — where the detector is further immersed in water. There, its reading corresponds to the dose in the medium at the initial point.[1] Otherwise, the measured curve would be shifted against the true dose distribution. Dosimetry protocols typically suggest a shift between 0.5[2] and 0.6 times[3,4] the cavity radius r of cylindrical ionization chambers to obtain the EPOM for measurements in photon beams.

Different methodologies to obtain EPOM values have been described in the literature.[5–9] Monte Carlo simulations have been carried out to compare the dose in water and the response of different detectors. The optimal shift was derived from these data.[5] Similarly, experimentally obtained curves were shifted against a reference curve for best agreement.[6] For the latter mentioned investigation, it was necessary to choose one detector, in that case a plane-parallel chamber, which was assumed to yield the correct depth dose curve. Another experimental method to determine the EPOM was carried out by bringing tissue phantom ratio (TPR) curves into alignment.[7] In that study, Gafchromic film was used as a reference.

The literature suggests that the position of the EPOM strongly varies among different chamber types.[6,7,10] While 0.5r seems to be a valid choice for a typical Farmer type ionization chamber, the values of 0.5r or 0.6r in current dosimetry protocols overestimate the shift necessary for smaller ionization chambers.[5,6] EPOM shifts for micro-ionization chambers as low as 0.1r to 0.2r have been reported.[10]

The EPOM depends slightly on the energy and field size. For a 25 MV photon beam, a reduced EPOM shift was found when the field size was increased from 10 × 10 cm^2 to larger field sizes.[5,10] For a 6 MV photon beam there have been contradictory observations, either a field size dependence[5] or an independence of the field size.[10] The EPOM shift increased at the lower beam quality.[10] Nevertheless, small differences in results as a function of field size obtained by Tessier and Kawrakow and by McEwen et al. suggest that one single EPOM shift per chamber over all beam qualities and field sizes can be applied in practice.[6,10]

Furthermore, a dependence of the EPOM shift on different chamber design parameters was found empirically.[5,10] Shorter chamber lengths and, given a fixed radius of the chamber, both a larger radius of the central electrode and a thicker chamber wall were shown to decrease the EPOM shift.[10] All

the dependencies on construction details impede the transfer of obtained EPOMs from one chamber type to a similar one, especially from one manufacturer to another or to even smaller chambers. This necessitates the generation of experimental data for new chamber types.

Recently, even smaller ionization chambers became available, such as the RAZOR Nano Chamber CC003 by IBA Dosimetry[11] with an active volume of 3 mm^3. In this work, we experimentally determined the effective points of measurement for different ionization chambers including several small field detectors with no data available so far. As the use of those smaller detectors will likely be restricted to small field dosimetry, this investigation focuses on field sizes between 2×2 cm^2 and 10×10 cm^2.

2. MATERIALS AND METHODS

The effective points of measurement for different ionization chambers were determined by comparing depth-ionization curves. The variation of water to air stopping power ratios with depth for an incident 6 MV beam is small[12] and normalized depth-ionization curves are comparable to normalized depth-dose curves for small ionization chambers in photon beams.[5] Therefore, measured ionization curves of photon beams are assumed to be equal to depth dose curves at least at depth beyond the dose maximum.[13] Ionization curves will be referred to as depth dose curves in the following. For the solid-state detectors, the normalized response is assumed to yield the depth dose curve as well. Depth dose curves obtained with different detectors were recorded and shifted to provide the best agreement with a reference curve measured with a plane-parallel chamber, which was assumed to yield the correct curve. The choice of the reference detector and its correct EPOM heavily influence the results. Therefore, the plane-parallel chamber results were validated by Gafchromic film measurements.

In this work, ionization chambers of different types and sizes were investigated: Farmer type FC65-G and the shorter FC23-C, scanning chamber CC13 and micro-chambers CC04, RAZOR chamber CC01 and RAZOR Nano Chamber CC003 (all IBA Dosimetry, Germany). Additionally, a microDiamond 60019 detector (PTW-Freiburg, Germany) and an unshielded silicon diode, the IBA RAZOR Detector, were included in the study for comparison. The reference curve was obtained with a PPC40 plane-parallel detector in nominal 4×4 cm^2 and 10×10 cm^2 fields and with a PPC05 detector (both IBA Dosimetry, Germany) in the nominal 2×2 cm^2 field. Detector details are listed in Table I.

Depth dose curves were measured for field sizes of 2×2 cm^2, 4×4 cm^2 and 10×10 cm^2 in an MP3 water phantom with the corresponding TANDEM electrometer and MEPHYSTO mc^2 software (PTW-Freiburg, Germany). The smallest step size possible with the MP3 phantom is 0.1 mm. The manufacturer states a reproducibility of 0.1 mm. The tank was set up at a source-to-surface distance (SSD) of 100 cm. A T-REF transmission chamber (PTW-Freiburg, Germany) was used to correct for linac output fluctuations.

TABLE I. Detectors used in this study and their dimensions according to manufacturer information.

Detector (Manufacturer)	Volume (cm^3)	Detector type	Radius of active volume (mm)	Length of active volume (mm)
FC65-G (IBA)	0.65	Farmer chamber	3.1	23
FC23-C (IBA)	0.23	Farmer chamber	3.1	9
CC13 (IBA)	0.13	Scanning chamber	3.0	5.8
CC04 (IBA)	0.04	Micro-chamber	2.0	3.6
CC01 (IBA)	0.01	Micro-chamber	1.0	3.6
CC003 (IBA)	0.003	Micro-chamber	1.0	2.0
PPC05 (IBA)	0.05	Plane-parallel chamber	4.95	0.6
PPC40 (IBA)	0.40	Plane-parallel chamber	8	2
RAZOR Detector (IBA)	–	Silicon diode	0.475	
microDiamond 60019 (PTW-Freiburg)	–	Diamond detector	1.1	

As depth dose curves measured with an in-room electrometer can be distorted due to scattered radiation reaching the electrometer and contributing to the signal, the electrometer was shielded by approximately 15 cm of lead.[14,15]

Each cylindrical ionization chamber was positioned with its axis perpendicular to the beam axis. The diode and microDiamond detector were positioned with their axes parallel to the beam axis. Plane-parallel chambers were positioned parallel to the beam axis. The central axis of the field was determined by profile scans. Zero depth was chosen in such a way that ionization chambers were positioned with their central chamber axis on the water surface. Solid state detectors were positioned in such a way that the top of the housing coincided with the water surface. The plane-parallel PPC40 chamber was positioned such that the back of the entry window coincided with the water surface, which is 1 mm behind the front face. A shift of the PPC05 of (-0.27 ± 0.05) mm from its reference point at the back of the entry window was obtained in the two larger fields to match the PPC05 curve with the PPC40 and the film curves. This shift was applied for the PPC05 to obtain the reference curve of the smallest field.

Bias voltages of 300 V were used for the ionization chambers. No biasing voltage was used for the diode and microDiamond detector. The dose per pulse of the linac was around 0.2 mGy at 5 cm depth and changed by approximately a factor two from the maximum to the deepest point of the acquired curves. At this low dose rate, saturation corrections do not exceed a few tenths of a percent for both plane-parallel chambers and the smallest micro-chamber[11,16] and were neglected as a result. The detectors, especially the small ionization chambers, were pre-irradiated at a minimum with the dose recommended by the manufacturers ($\leq$10 Gy) to stabilize the detector response.

Measurements were done using a Primus linac (Siemens, Germany) with a nominal acceleration voltage of 6 MV ($TPR_{20,10}$ = 0.678). Fields are shaped with leaves in cross-plane and with jaws in the inplane direction. All field sizes stated here are nominal field sizes, which are defined at 100 cm distance from the focus.

The scan direction was always toward the water surface. The step width between the discrete measurement points was 0.5 mm, except in the vicinity of the dose maximum, where it was improved to 0.1 mm. The integration time per measurement point was adapted to the detector sensitivity to increase the signal-to-noise ratio and ranged from 0.2 to 1.0 s. The TANDEM electrometer measures current in intervals of 1 ms. For the micro-ionization chambers and the PPC05, measurements were repeated after switching the polarity of the biasing voltage and repeating pre-irradiation. Polarity effects for the Farmer and PPC40 were negligible for the considered depths until 8 mm, so measurements were only carried out at positive polarity. Between two and five curves per detector and field size were obtained – each on a different day with a completely independent setup of the water tank to determine the repeatability of the results.

The measured curves were further processed using MatLab (MathWorks, USA). Because the high gradient regions were measured with a point spacing of 0.1, the 0.5 mm intervals between measurement points elsewhere were interpolated linearly to get the same spacing. The curves were not smoothed before the analysis. Where applicable, the curves at positive and negative biasing voltage were averaged. The curves were normalized to the signal at 10 cm depth. When curves were shifted by a distance Δz during the subsequent analysis, the normalization depth became 10 cm + Δz. Next, the relative signals for each detector *Det* were compared against those obtained with the reference detector *Ref* quantifying and minimizing their deviation of relative doses over all depths z_i larger than 8 mm as χ^2:

$$\chi^2 = \sum_{z_i} \left[\frac{S_{Det}(z_i + \Delta z) - S_{Ref}(z_i)}{S_{Ref}(z_i)} \right]^2 . \quad (1)$$

Numerically, the value of Δz is determined such that χ^2 is minimized. The obtained Δz yields the shift that provides the best agreement between the two curves, hence the EPOM shift. Due to the discrete spacing of the included data, the type A uncertainty of Δz is 0.05 mm. Shifts Δz were obtained for all combinations of curves measured with the respective detector and the reference detector. Those values were averaged per field size. Secondly, the values of all combinations in all field sizes were averaged to yield a single shift Δz per detector. The uncertainty of the mean was determined as the standard deviation of the shifts of different detector combinations divided by the square root of the number of measurements. The FC65-G curves obtained in the 2 × 2 cm^2 field were excluded, because the diameter of the active volume is too large compared with the field size.

The sign of Δz is chosen such that positive Δz means that the detector is moved away from the radiation source, while a negative Δz means that the detector is moved further toward the radiation source (Fig. 1). To exclude an effect of the large differences between the detector signals in the build-up region on the obtained EPOMs, z_i were restricted to depths beyond 8 mm.

In order to validate the chosen measurement points of the PPC40 chamber, depth dose for field sizes 4 × 4 cm^2 and 10 × 10 cm^2 were measured with EBT3 film. Three pieces of film per depth (1, 3, 5, 7, 9, 11, 13, 15, 17, 20, 30, 40, 50, 150, and 200 mm depth) were consecutively irradiated in the same setup in the water phantom. The film was fixed to a custom-built PMMA frame holder, leaving the center of the film in contact with water and minimizing the perturbation from the holder (Fig. 2). Film positioning was done visually at the water surface. After 48 h the films were scanned using an EPSON Expression 1100XL scanner with a transparency unit. Optical density was converted into dose using FilmQA Pro software (Ashland, USA) taking into account all three color channels.[17] Dose values per depth were averaged and a depth dose curve was fitted to the data using a function established in fitting TPRs.[18] Film and the PPC40 curves were then compared for both field sizes following the same steps as described above for the comparison of different detectors.

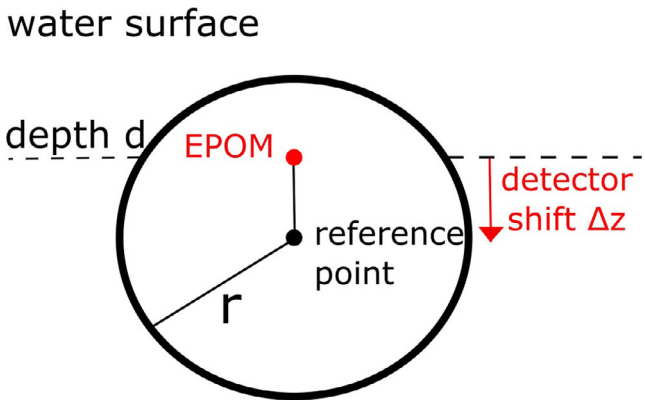

FIG. 1. Schematic illustration how the effective point of measurement (EPOM) is defined. The cylindrical ionization chamber is positioned with its EPOM at a certain depth. This position is reached by shifting the reference point in the detector center by a distance Δz away from the radiation source. [Color figure can be viewed at wileyonlinelibrary.com]

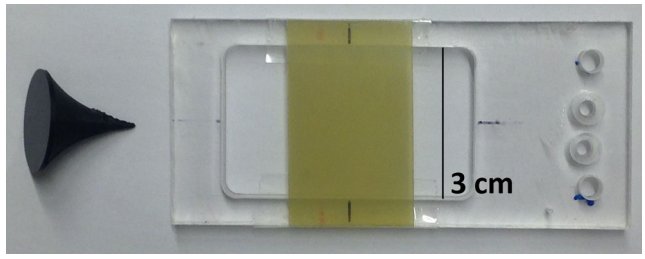

FIG. 2. Holder used for the film measurements (right). The film is attached to the frame on two sides while its center is surrounded by water only. The holder can be attached to the water phantom. Cone used to adjust detector positions relative to the water surface (left). [Color figure can be viewed at wileyonlinelibrary.com]

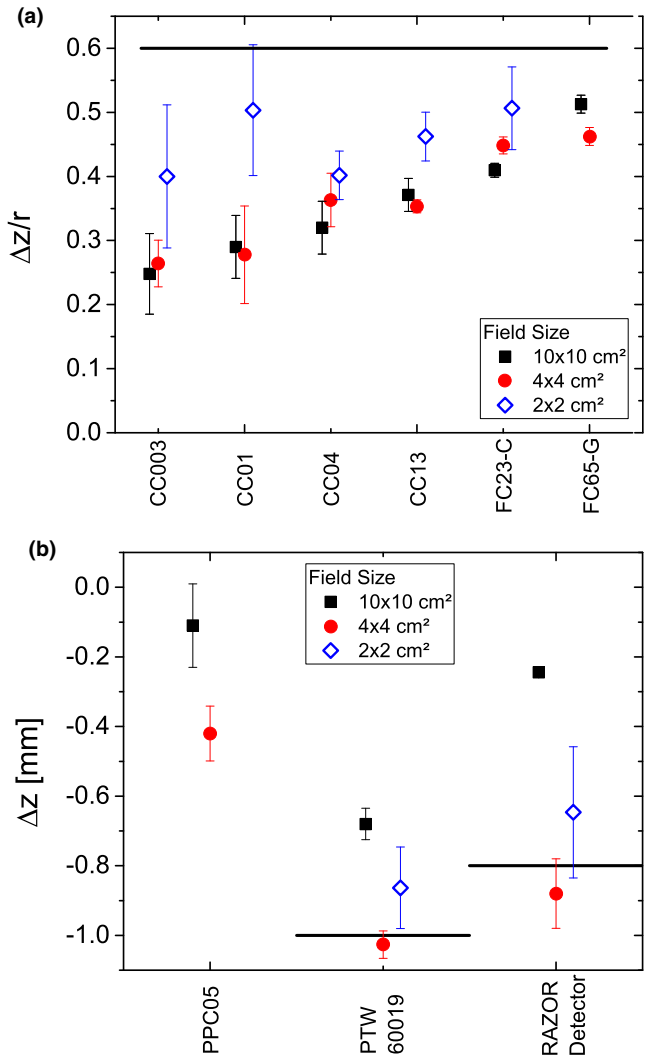

FIG. 3. Experimentally obtained effective point of measurement for different detectors. (a) Displayed is the fraction of the cavity radius, which cylindrical ionization chambers need to be shifted from their central axis. (b) The absolute shift for the plane-parallel PPC05 is measured from its reference point at the back of the entry window, and those for the solid state detectors indicate the distance from their front face. A positive sign indicates a shift away from the radiation source. Cylindrical ionization chamber volumes increase from left to right. Thick lines represent the value of 0.6r recommended in most dosimetry protocols for the ionization chambers in (a) and the position of the measurement point relative to the detector tip as indicated by the manufacturers for the solid state detectors in (b). Error bars represent the uncertainty of the mean. In some cases the symbol size exceeds the error bars. [Color figure can be viewed at wileyonlinelibrary.com]

3. RESULTS

The determined shifts to obtain the EPOMs for the different detectors for the three studied field sizes are shown in Fig. 3. The shifts for the Farmer type chambers are approximately 0.5r. The necessary shifts decrease for smaller chambers.

EPOM shifts were clearly increasing for the 2×2 cm^2 field compared to the two larger fields investigated. In addition, shifts for the solid-state detectors and the PPC05 in the 10×10 cm^2 field differed from the smaller field sizes. For practical purposes, the very small and uncertain field size dependence of the EPOMs can be neglected. The averaged shifts over all field sizes for the different detectors are given in Table II. Examples of EPOM shifted depth dose curves for different detectors are shown in Fig. 4.

TABLE II. Shifts from the central chamber axes for ionization chambers and from the top of the solid state detectors to the effective point of measurement averaged over three field sizes between 2×2 cm^2 and 10×10 cm^2, stated both in mm and as a function of detector inner radius, where applicable. Stated uncertainties represent one standard deviation of the mean. The last column shows the difference between 0.6r and Δz.

Detector	Shift Δz (mm)	Shift Δz/r	0.6r − Δz (mm)
FC65-G	1.51 ± 0.04	0.49 ± 0.01	0.35
FC23-C	1.41 ± 0.04	0.45 ± 0.01	0.45
CC13	1.19 ± 0.04	0.40 ± 0.01	0.61
CC04	0.72 ± 0.05	0.36 ± 0.03	0.48
CC01	0.36 ± 0.04	0.36 ± 0.04	0.24
CC003	0.30 ± 0.04	0.30 ± 0.04	0.30
RAZOR detector	−0.59 ± 0.07		
microDiamond 60019	−0.86 ± 0.04		

The PPC40 chamber and the film yielded very similar curves (Fig. 4). Shifts for the PPC40 against the film were (-0.1 ± 0.1) mm in the 10×10 cm^2 field and (0.04 ± 0.1) mm in the 4×4 cm^2 field. The EPOM of the PPC05 was found to require a shift of 0.27 mm from its reference point to agree with the PPC40 [average of values, see Fig. 3(b)]. When the PPC05 was shifted by this distance, the curves obtained with this chamber in the 2×2 cm^2 field agreed with film within the uncertainties at depths larger than 9 mm. Over that, shifts for the PPC05 against the film were (-0.2 ± 0.3) mm averaged over all field sizes and approximately -0.3 mm in the 2×2 cm^2 field.

4. DISCUSSION

All resulting effective points of measurements were smaller than 0.5-times the cavity radius. This agrees with the observations reported in the literature (Fig. 5). Values for Farmer type chambers close to 0.5r have been reported, for example, values between 0.483r and 0.512r depending on the field size and beam quality for a PTW 30013.[10] A decrease of the shifts for the smaller chambers was reported in the literature.[10] This trend continued even for the smallest studied detectors, the CC01 and CC003 with very small dimensions and collecting volumes down to 3 mm^3. Such a reduction was to be expected, as the EPOM shift was shown to depend on the cavity length, central electrode radius and the cavity wall thickness.[10] Both, the ratio of the radius of the central electrode to the chamber radius and the wall thickness compared to the chamber radius increase with decreasing chamber radius. Therefore, the EPOM shift decreases. The EPOM also decreased from the Farmer chamber FC65-G to the FC23-C, which both have the same radius but the first one is longer and has a graphite outer electrode while the latter is composed of C552.

Even though the authors are not aware of any published EPOM data for most of the studied chambers, the obtained

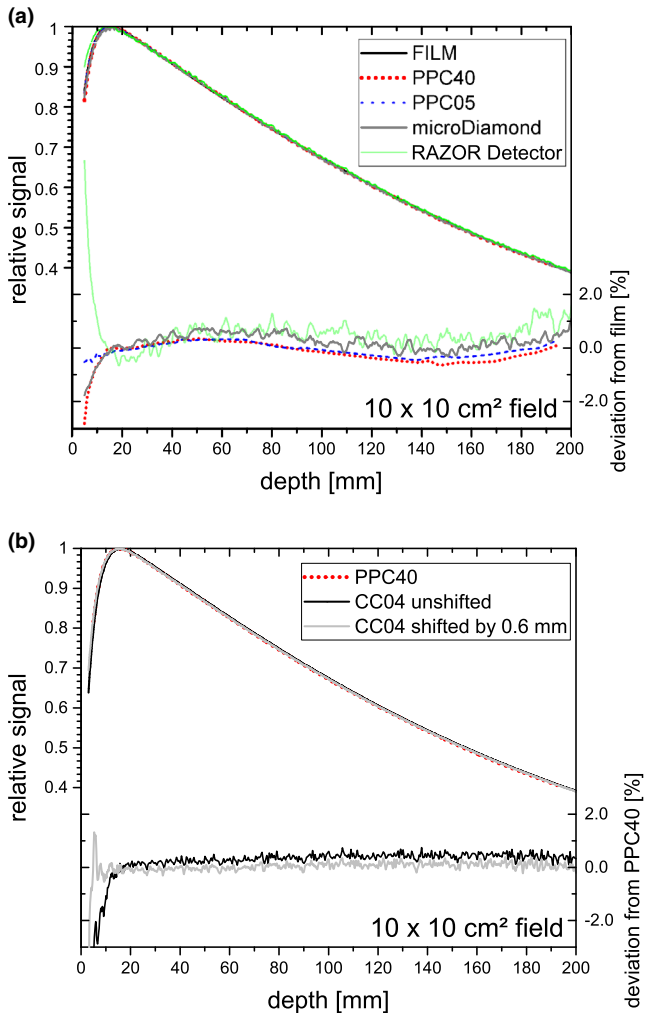

FIG. 4. (a) Example curves measured with different detectors in a 10 × 10 cm^2 field after the shift has been applied (left scale). While EBT3 and the ionization chamber curves are almost indistinguishable, the diode curve cannot be aligned at all depths. Deviations between the shifted curves and the film are shown below (right scale). The curves were smoothed for display in this figure and for analysis. (b) Example curves of a CC04 chamber unshifted with the depth set at its reference point and an additional curve shifted by Δz, which takes the value of 0.6 mm as derived from the 0.3r shift for the respective field size in Fig. 3(a) and the chamber radius of 2 mm (both curves displayed with the left scale). The difference between these curves and the reference PPC40 is displayed (right scale). [Color figure can be viewed at wileyonlinelibrary.com]

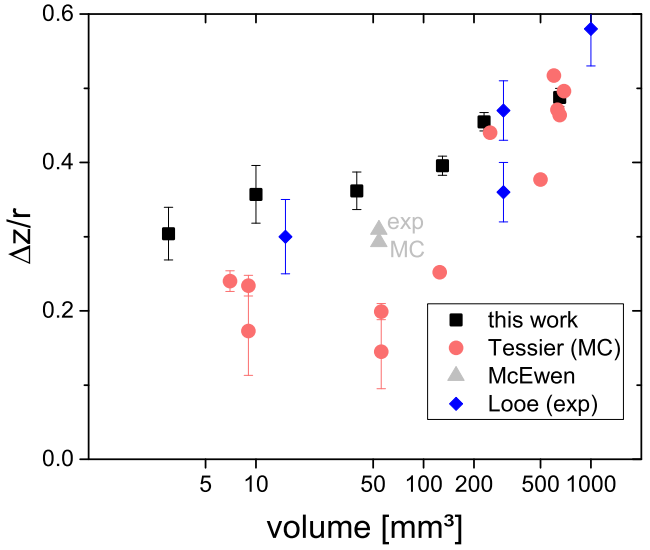

FIG. 5. Comparison of the obtained effective point of measurement shifts averaged over all field sizes with existing literature data for chambers by different manufacturers. Data from Tessier is simulated for a beam quality of 6 MV,[10] from McEwen measured and simulated for 25 MV[6] and from Looe measured in 6 and 15 MV and averaged,[7] all for a field size of 10 × 10 cm^2. [Color figure can be viewed at wileyonlinelibrary.com]

shifts for the micro-chambers seem reasonable in comparison to measurements performed with other small cylindrical ionization chambers from different manufacturers in photon beams (see Fig. 4).[6,7,10] For the PinPoint chamber PTW 31006 with a volume of 15 mm^3 a shift of (0.30 ± 0.05)r was reported.[7] In this work we found (0.36 ± 0.04)r for the CC01 with 10 mm^3 volume. For Exradin A16 and A14 chambers with active volumes of 7 and 9 mm^3 shifts of approximately 0.2r were found.[10] In this work we found (0.30 ± 0.03)r for the CC003 with 3 mm^3 volume. While the volume is certainly one of the parameters that plays a role, it has been shown that other design parameters influence the position of the EPOM, especially chamber length and the details of the central electrode and chamber wall.[10] Moreover, a reduction of the EPOM shift with increasing field size was reported for larger field sizes,[5,10] which can account for the systematically higher values in this work. Here, averages between three small field sizes are provided while the literature data (Fig. 4) is for 10 × 10 cm^2 fields. The EPOM can be expected to decrease with the amount of scatter in a field and vanish in the limit of isotropic radiation.[10] For the smallest studied field size, lateral charged particle equilibrium is reduced and electrons are mainly impinging from the front. The trend of decreasing EPOM with field size is in agreement with a field size dependence observed in the literature, albeit between the much larger 30 × 30 cm^2 and 10 × 10 cm^2 fields.[5] Given the uncertainties associated with the different measurement points in Fig. 3, the results from all three field sizes were grouped together and stated as one shift that is independent of field size.

Despite the good agreement between the measured data and the literature, there are a couple of critical choices in the procedure. One is the choice of the cut-off in the build-up region, which influences the results. McEwen et al. already discussed this point and its consequences.[6] For their work, they chose the minimum possible depth to completely immerse the studied detector. Since detector differences were considerable near the surface and this part of the curve would disturb the results, we chose a minimum depth of 8 mm for a measurement point to be included in the analysis. Relative depth doses for all studied cylindrical detectors at a depth of 8 mm differed at maximum approximately 1% from one another. Making this choice, the depth of dose maximum was fully included in the optimization.

Moreover, it has been stated that the experimental determination of EPOMs is difficult and that a positioning precision

of 0.1 mm is necessary to compare different thimble chambers.[5,6] Positioning detectors at the water surface based on reflection images may introduce systematic errors[19,20] and the surface tension of the water may obscure the initial depth setting, especially for the plane-parallel chambers. Therefore, for the plane-parallel chambers, the initial depth was carefully set and verified with a 3D-printed, light plastic cone (Fig. 2) of known length and a density just slightly above water density placed on top of the detector as a positioning tool. It had a very sharp tip, which made it possible to see when the tip approached the surface while simultaneously decreasing all the concerns about the surface tension. The cylindrical chambers were also positioned visually at the water surface, which was verified by the following alternative approach. Siebers et al.[20] and Ververs et al.[19] proposed calculating the first derivative of the depth dose curve and finding the maximum. This point indicates the position when the wall of a cylindrical detector just reaches the water surface. Our positioning of the cylindrical chambers was consistent with that approach, as it yielded the same shift for the CC13 tested as an example of a cylindrical chamber. After repeating the positioning multiple times, we have confidence in the initial depth setting with respect to the water surface and claim that it is precise within approximately 0.1 mm.

The procedure to derive the EPOMs further relies on the assumption that the curves obtained with the reference detectors represent the true depth dose curve. The results obtained heavily depend on the choice of the EPOM of the parallel-plate chambers. We verified the choice of the PPC40 chamber's position against EBT3 measurements and did not find a necessary shift for the used chamber and beam quality. Remaining differences between the reference detector and the film showed a non-monotonic depth dependence and had a maximum deviation of 0.5% at any depth. Depth dependent differences between film and the other detectors may be caused by an EPOM changing with depth due to several factors, such as changing field sizes due to beam divergence, angular dependency of the detector response, beam hardening and the lack of backscatter at large depths close to the exit side of the phantom. All these effects are small contributions and remain to be investigated in detail. Therefore, we kept the back of the entry window as the EPOM for this study. This is in contrast to some of the observations in the literature. For the PTW Roos chamber, which is similar but not identical in design, a shift of the EPOM of 0.6 mm into the chamber cavity was reported.[7] Simulations of the IBA PPC40 in electron beams suggest a shift of 0.39 mm into the cavity.[21]

In our study, it was necessary to change the reference detector for the smallest field. A shift of (-0.27 ± 0.05) mm between the curves with the PPC05 detector and the PPC40 detector was noticed in the 4×4 cm^2 and 10×10 cm^2 fields when both detectors were positioned with their reference points, the back of the entry window, at the measurement depth. The position of the PPC05's EPOM in the 2×2 cm^2 field was set accordingly and validated against depth dose curves on EBT3 film. In the literature, for the IBA PPC05 in a 10×10 cm^2 electron beam a 0.58 mm shift into the cavity was reported, while the PPC40 required a shift of 0.39 mm,[21] implying a relative shift of 0.21 mm. This is very close to the 0.27 mm used in this work, despite the limited comparability of these data from different beam types.

Several influence parameters contribute to the uncertainties of the determined EPOMs: Water evaporation, the initial placement of the chamber axis on the surface, the phantom motor step size and reproducibility, the correct SSD, inclination of the water tank or noisy curves. As the phantom was set up several times and as the curves were measured multiple times per detector, all these points are assumed to be included in the uncertainty of the mean.

Polarity effects can be an issue with ionization chambers. There were very little changes of the polarity effects as a function of depth. Relative depth dose curves changed by as little as 0.5% for the CC01 and the CC003 past 15 mm depth and by 2% and 3%, respectively, until 8 mm depth. For the other detectors, relative changes could not be observed or were of the order of statistical fluctuations. However, towards the surface—which is not included in this analysis—the differences increased further. All these data were obtained with a lead shielding of the in-room electrometer in place, being necessary to eliminate an interfering signal produced in the electrometer itself.[15]

The different volumes of different detectors can lead to volume averaging influencing the shape of the measured depth dose curves in smaller fields. This is especially a concern for the 2×2 cm^2 field, in which the PPC40 and FC65-G were not used for this reason. For the remaining chambers, the effect on the depth dose curves was estimated from beam profiles recorded on film at different depths and changes were at most 0.3% for the PPC05 at 8 mm depth. For the detectors with smaller dimensions the effect was even smaller.

The RAZOR Detector (diode) yielded depth dose curves with a slightly different slope compared to the reference detector curve [Fig. 4(a)]. The difference between the slopes was largest in the 10×10 cm^2 field. The observed EPOM shift for that field size was smaller than for the two other studied fields (Fig. 3). Diode overresponse due to the increased silicon cross-sections to low-energy photons, as found in large fields and at large depths, is a known limitation of such detectors.[22,23] It changes the slope [Fig. 4(a)] and, therefore, influenced the determination of the EPOM, based on the depth dose curves as a whole. This is a possible reason for the RAZOR Detector showing a result in the 10×10 cm^2 field that deviates from the shift expected according to manufacturer information. It also shows the limitation of the analysis procedure and the EPOM concept. If a detector shows a depth dependent response, a simple EPOM shift is not sufficient to achieve the true depth dose function. At the 10×10 cm^2 field size, the microDiamond curves also show a slope that slightly deviates from the curves recorded with the reference detectors, resulting in smaller EPOM shifts than at the smaller field sizes [Fig. 4(a)].

This study concentrated on field sizes below 10×10 cm^2. A field size dependence of the EPOM has been shown for some chambers especially in much larger

fields[5,10] and seems reasonable to exist also at the smaller field sizes. Since the results obtained for the three different field sizes agreed within the uncertainties, a single EPOM per detector was stated. Beam quality is known to influence the EPOM as well.[10] However, the reported differences between 6 and 25 MV are marginal and for most detectors the values are identical within the uncertainties. The Linac available for this experiment provided only one photon energy, so the investigation had to be limited to 6 MV. The tabulated 6 MV EPOMs are likely a better estimate also at other beam qualities compared to the canonical 0.5r or 0.6r until the investigation has been extended to other beam qualities.

The practical impact of applying the experimentally obtained EPOMs rather than the classical 0.5r or 0.6r choice might be limited given that typical shifts are between 0.2 and 0.4 mm. Only very few dosimetry protocols[2] ask for an EPOM shift to be explicitly performed for reference dosimetry—and very small chambers with volumes below 50 mm^3 are not recommended for the purpose of reference dosimetry anyway.[24] However, in other protocols,[3,13] the choices of the EPOM are implicitly included in the beam quality conversion factors.[25] Moreover, the small shifts lead to large effects when measuring depth dose curves in the high gradient build-up region: Shifting depth dose curves by 0.4 mm introduces a 2% change of the depth dose curve at 5 mm depth and a 5% change at 3 mm depth.

5. CONCLUSIONS

We determined the EPOM in small MV photon beams for several detectors, particularly for small ionization chambers with active volumes down to 3 mm^3. The resulting shifts were different for different detectors, but were comparable for each detector in all three studied field sizes from 2 × 2 cm^2 to 10 × 10 cm^2. Therefore, the results were averaged to one EPOM per detector valid for every field size. For the smaller ionization chambers 0.5r or 0.6r are not the appropriate choices. These results should be considered when selecting the EPOM for detectors as it can be especially important when measuring depth dose curves.

ACKNOWLEDGMENTS

The authors thank IBA Dosimetry for the loan of several of their small field detectors. Sonja Wegener was supported by DFG grant SA 481/10-1. The authors thank Barbara Herzog for carrying out the analysis to estimate the effect of volume averaging on relative depth dose curves and Gary Razinskas for carefully reading the manuscript.

CONFLICT OF INTEREST

There is no conflict of interest to declare.

[a]Author to whom correspondence should be addressed. Electronic mail: wegener_s1@ukw.de.

REFERENCES

1. Andreo P, Burns DT, Nahum AE, et al. *Fundamentals of Lonizing Radiation Dosimetry.* Weinheim, Germany: Wiley-VCH; 2017.
2. 6800-2:2008-3, D., *Dosismessverfahren nach der Sondenmethode für Photonen- und Elektronenstrahlung - Teil 2: Dosimetrie hochenergetischer Photonen- und Elektronenstrahlung mit Ionisationskammern*; 2008.
3. Almond PR, Biggs PJ, Coursey BM, et al. AAPM's TG-51 protocol for clinical reference dosimetry of high-energy photon and electron beams. *Med Phys*. 1999;26:1847–1870.
4. IAEA, Dosimetry of Small Static Fields Used in External Beam Radiotherapy, in *Technical Reports Series No*. 483. Vienna: International Atomic Energy Agency; 2017.
5. Kawrakow I. On the effective point of measurement in megavoltage photon beams. *Med Phys*. 2006;33:1829–1839.
6. McEwen MR, Kawrakow I, Ross CK. The effective point of measurement of ionization chambers and the build-up anomaly in MV x-ray beams. *Med Phys*. 2008;35:950–958.
7. Looe HK, Harder D, Poppe B. Experimental determination of the effective point of measurement for various detectors used in photon and electron beam dosimetry. *Phys Med Biol*. 2011;56:4267–4290.
8. Lacroix F, Guillot M, McEwen M, et al. Extraction of depth-dependent perturbation factors for parallel-plate chambers in electron beams using a plastic scintillation detector. *Med Phys*. 2010;37:4331–4332.
9. Lacroix F, Guillot M, McEwen M, et al. Extraction of depth-dependent perturbation factors for silicon diodes using a plastic scintillation detector. *Med Phys*. 2011;38:5441–5447.
10. Tessier F, Kawrakow I. Effective point of measurement of thimble ion chambers in megavoltage photon beams. *Med Phys*. 2010;37:96–107.
11. Reggiori G, Stravato A, Mancosu P, et al. Small field characterization of a Nanochamber prototype under flattening filter free photon beams. *Phys Med*. 2018;49:139–146.
12. Eklund K, Ahnesjö A. Fast modelling of spectra and stopping-power ratios using differentiated fluence pencil kernels. *Phys Med Biol*. 2008;53:4231–4247.
13. IAEA. Absorbed Dose Determination in External Beam Radiotherapy. Technical Reports Series. Vienna: International Atomic Energy Agency; 2000.
14. Sarkar V, Wang B, Zhao H, et al. Percent depth-dose distribution discrepancies from very small volume ion chambers. *J Appl Clin Med Phys*. 2015;16:432–442.
15. Wegener S, Sauer OA. Electrometer offset current due to scattered radiation. *J Appl Clin Med Phys*. 2018;19:274–281.
16. Bruggmoser G, Saum R, Schmachtenberg A, et al. Determination of the recombination correction factor kS for some specific plane-parallel and cylindrical ionization chambers in pulsed photon and electron beams. *Phys Med Biol*. 2007;52:N35–N50.
17. Micke A, Lewis DF, Yu X. Multichannel film dosimetry with nonuniformity correction. *Med Phys*. 2011;38:2523–2534.
18. Sauer OA, Wilbert J. Functional representation of tissue phantom ratios for photon fields. *Med Phys*. 2009;36:5444–5450.
19. Ververs JD, McEwen MR, Siebers JV. Quantitative ionization chamber alignment to a water surface: performance of multiple chambers. *Med Phys*. 2017;44:3839–3847.
20. Siebers JV, Ververs JD, Tessier F. Quantitative ionization chamber alignment to a water surface: theory and simulation. *Med Phys*. 2017;44:3794–3804.
21. Muir BR, Rogers DW. Monte Carlo calculations of electron beam quality conversion factors for several ion chamber types. *Med Phys*. 2014;41:111701.
22. Sauer OA, Wilbert J. Measurement of output factors for small photon beams. *Med Phys*. 2007;34:1983–1988.
23. Griessbach I, Lapp M, Bohsung J, et al. Dosimetric characteristics of a new unshielded silicon diode and its application in clinical photon and electron beams. *Med Phys*. 2005;32:3750–3754.
24. McEwen M, DeWerd L, Ibbott G, et al. Addendum to the AAPM's TG-51 protocol for clinical reference dosimetry of high-energy photon beams. *Med Phys*. 2014;41:041501.
25. Zakaria A, Schuette W, Younan C. Reference dosimetry according to the New German protocol DIN 6800–2 and comparison with IAEA TRS 398 and AAPM TG 51. *Biomed Imaging Interv J*. 2011;7:e15.